Paper ID ICLASS06-283

SPRAY FEATURES INVESTIGARED BY GSV: A NEW PLANAR LASER TECHNIQUE

G. Pan[1], J. Shakal[1], W. Lai[1], R. Calabria[2], P. Massoli[2]
[1.] TSI Inc., Shoreview, MN 55126 USA
gpan@tsi.com, jshakal@tsi.com, wlai@tsi.com
[2.] Istituto Motori - CNR, Naples, Italy
p.massoli@im.cnr.it, r.calabria@im.cnr.it

ABSTRACT A spatial technique providing global size and velocity data over a two-dimensional region of a spray is often preferred for rapid optical characterization of sprays. The Generalized Scattering Imaging (GSI) approach for droplet sizing, based on both the Lorenz-Mie theory and the Finely Stratified Sphere Scattering Model can be applied to both homogenous droplets and inhomogeneous and/or absorbing droplets. A new system has been developed using the GSI approach, with the capability to measure the velocity and size of droplets with non-uniform and/or varying refractive index, even in regions of high particle number density. A windowed FFT based approach was used to identify the presence and location of a droplet oscillation pattern, and an optimized frequency-based algorithm was used to extract the droplet size. A two-frame tracking algorithm was devised to measure the velocity of droplets from the two consecutive image frames. The size range and droplet concentration limits were investigated using simulated out-of-focus images. A maximum measurable diameter range from 10μm to 600μm was obtained for the range of magnification and defocus recommended here. The maximum droplet concentration is expected to be about 3000 #/cc. Sizing accuracy was verified using monodisperse droplets and a graded index optical fiber. Results obtained for a swirl type pressure atomizer operating on water and fuel oil depicted well the near-nozzle spray angle and diameter characteristics in various parts of the spray structure. Velocity vector maps were obtained, and when combined with the size measurements, size-velocity correlations were constructed. Data was also acquired for a gasoline direct injector (G-DI) operating at a limited range of conditions, and the resulting droplet size distributions were analyzed.

Keywords: Global Measurement, Interferometric Sizing, GSV, GSI, Image Based Sizing

1. Introduction

In practical industrial systems (e.g., combustion and drying processes) or in simulation test rigs (e.g., in icing tests to simulate atmospheric droplet freezing) droplets may undergo fast and significant variation of diameter, composition, and, hence, refractive index. Spray characterization is based on the analysis of the temporal and spatial evolution of droplet size and velocity. Ensemble light scattering techniques are able to perform measurements in very dense sprays, up to the limit of the multiple scattering, but they furnish only a moment of the droplet size distribution, with no information on velocity. Point techniques, like phase Doppler, have good spatial resolution, but measurement over a two-dimensional region requires the spray to remain invariant for a significant period of time. Pulsed sprays are always unsteady, by their nature. Instrument response also depends on the droplet refractive index. A spatial technique providing instantaneous global size and velocity over a two-dimensional region of the spray would thus be preferred. However, application of global sizing techniques to sprays is often limited by the number concentration of droplets, especially when the optical method is based on identification of every droplet in the image.

It is well known that light scattered by small droplets is characterized by strong angular oscillations. Early research has found that the oscillations have almost uniform angular spacing that is inversely proportional to the droplet diameter [1]. The idea of using out-of-focus imaging to record the oscillations for droplet sizing was first introduced by Ragucci et al. in 1990 [2]. Today out-of-focus imaging has become the standard imaging method in many commercial 2D droplet sizing systems.

Recently, Massoli and Calabria developed Generalized Scattering Imaging (GSI), a comprehensive approach for droplet sizing based on out-of-focus imaging [3]. It is called "Generalized Scattering Imaging" because it is based on both the Lorenz-Mie theory [1] and the Finely Stratified Sphere Scattering Model [4] and therefore can be applied to not only homogenous droplets but also inhomogeneous and/or absorbing droplets. One important aspect of GSI is that at a 60° scattering angle, the oscillation spacing of the scattered light is most insensitive to refractive index. For radially inhomogeneous droplets or absorbing droplets, the diameter is given by $D = 1.129 \cdot \lambda / \Delta\vartheta$ where $\Delta\vartheta$ is the angular oscillation spacing and λ is the light wavelength in vacuum. The same relationship also applies to homogenous droplets. However, if the refractive index is known, a more accurate coefficient (instead of 1.129) can be found based on calculated scattering data.

Based on Generalized Scattering Imaging a new droplet analysis system incorporating novel algorithms of sizing and velocity has been designed and developed. The objective of the new system is to have the capability to measure droplets with non-uniform and/or varying refractive index even in regions of high particle number

density, such an in certain types of fuel sprays. Since droplet velocity is a desirable result for flux calculation, the system also needs to provide simultaneous velocity and size measurement. Incorporating the measurement concept of PIV, the new system employs a single camera operating in the PIV capture mode to capture two consecutive image frames of the defocused droplets with small time separation between the images. Since the droplets travel a certain distance in the time interval between the two frames, the velocity of the droplets can be measured. Hence the new system provides the capability to simultaneously measure the droplet size and velocity in a 2D spatial region of the spray, using a single camera. The major hardware components for the system are very similar to those of a PIV system, employing a laser for light sheet illumination, a synchronization unit for timing control, a CCD camera with PIV capture capability and software for image capture and analysis. In order to accommodate for droplets in non-stationary conditions such as evaporating or burning sprays, the system records oscillations at a 60° scattering angle to take advantage of GSI. Image distortion due to 60° imaging is corrected by a new geometric correction method. As a result, the calibration required by the system is very simple, and the magnification factor before defocusing is the only calibration required. To allow for measurements in higher number density environments, a slit in front of the camera lens is employed to block all but a narrow string of the original out-of-focus image [5]. This not only reduces the possibility of oscillation pattern overlap, but also improves the quality of recorded oscillations. The system also incorporates a novel windowed FFT algorithm for fast and fully automated sizing identification, and a special tracking scheme for the velocity measurement. Details of the system configuration, the analysis algorithms and the system characteristics are described in later sections. The system was used for a variety of tests to determine its performance limits and robustness. Typical test results for monodisperse droplet measurement and water sprays are also presented in later sections.

2. Description of the System

Figure 1 shows the hardware recording setup. The laser source is a 532 nm double-pulsed Nd:YAG laser. This allows droplet motion to be 'frozen' in time, whether the spray is steady or transient (pulsed). A high-resolution CCD camera (12bit) is installed at 60° scattering angle and focuses at a plane slightly away from the light sheet. A slit is placed in front of the lens to isolate a portion of the oscillation pattern. A sample out-of-focus image of water spray is shown in Figure 2.

From out-of-focus images like the one shown in Figure 2, the oscillation spacing in pixels can be obtained. The simplest way to convert the spacing in pixels to the angular spacing $\Delta\vartheta$ is by using the equation $\Delta\vartheta = M\delta/\Delta z \cdot n$, where M is the magnification (after defocusing), Δz is the defocusing distance, δ is the pixel size, and n is oscillation spacing in pixels. Since the 60° angle of the camera does not focus at a plane parallel to the light sheet, the defocusing distance and magnification are not uniform across the image, and a correction is required.

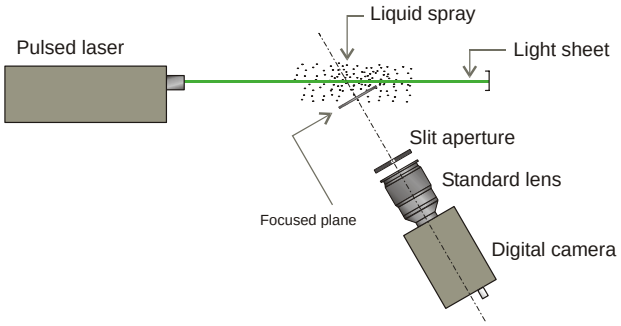

Figure 1: Recording hardware arrangement.

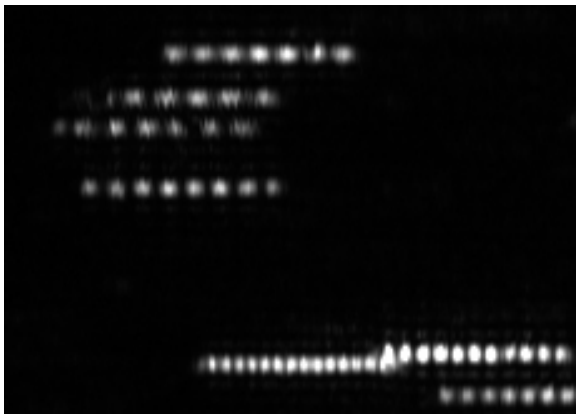

Figure 2: Portion of an out-of-focus spray image (size shown is 228 × 162 pixels).

Figure 3 illustrates the defocused imaging configuration. Using geometric optics, the following equations for defocusing distance dz and magnification M can be obtained:

$$dz = dz_0 + (1+M_0)\cdot f\cdot\sin\alpha\cdot[\sin\alpha - \cos\alpha\cdot\tan(\alpha+\beta)] \quad (1)$$

$$M = M_0 - (1+M_0)\cdot\sin\alpha\cdot[\sin\alpha - \cos\alpha\cdot\tan(\alpha+\beta)] \quad (2)$$

where α is the angular position and β is the Scheimpflug angle. The nominal value of dz_0 and M_0 are calculated using the actual defocusing translation Δz and the pre-defocusing magnification M (from the calibration). Figure 4 shows measured results before and after the geometric correction was applied. The test was done using monodisperse droplets recorded in different horizontal positions. Similar results are also obtained in tests where a thick glass window is placed between the droplet field and the camera, indicating that the algorithm is insensitive to this type of change in optical path and effective focal length.

3. Processing Algorithms

3.1 Sizing algorithm

The sizing algorithm is designed to extract the droplet size and position from the oscillation patterns present in out-of-focus images. Generally, the sizing algorithm is composed of two steps: (a) identifying each oscillation pattern to determine the droplet location; and (b) analyzing each pattern to determine the droplet size.

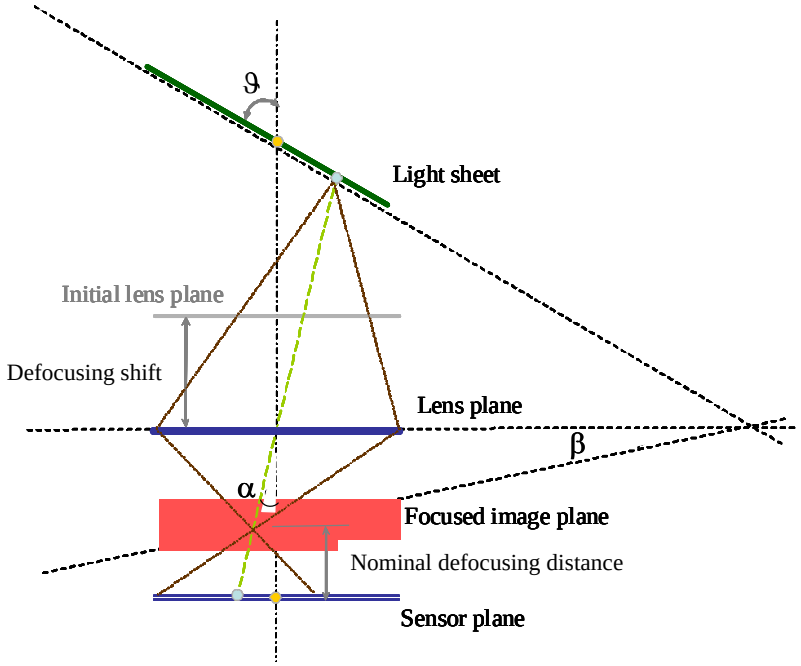

Figure 3: Defocused imaging configuration.

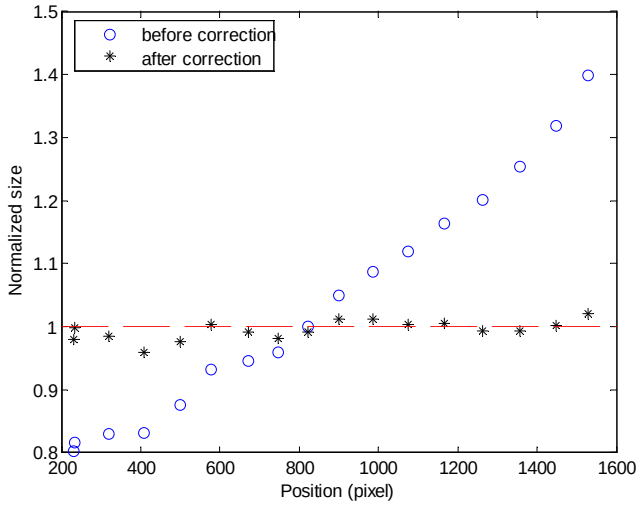

Figure 4: Results of geometric correction.

Edge detection is the most commonly used method in identifying uncompressed (circular) oscillation patterns [6, 7]. For compressed or truncated (rectangular) patterns, Maeda et al. used low-pass filtering to convert the oscillations to 1D Gaussian pattern, for which the peak position is considered to be the center of the oscillation pattern [8]. A novel algorithm based on a windowed FFT technique is used here, in order to provide a more robust, user-friendly method of identification of the oscillation patterns [9]. The algorithm has four steps: (1) First the image is scanned vertically to obtain a 1D intensity profile along the horizontal direction in each scan. (2) Then the windowed FFT of the 1D data is computed at each horizontal position to obtain the space-frequency distribution of power spectra. (3) The center and boundaries of valid oscillations are found in the power spectra. Valid oscillation patterns always have a single dominant frequency while dubious structures such as non-spherical particles, multi-droplet effects, or bad pixels having no dominant frequency, are all rejected. The use of 2D power spectra also improves identification of overlapped patterns. Even if two patterns overlap in the spatial domain, they are separated in the frequency domain as long as the oscillation spacings are different. (4) After pattern identification, individual patterns are extracted from raw images for frequency analysis to obtain the oscillation spacing. This can be done either in space domain by autocorrelation or in frequency domain by Fourier transform. We found Fourier transform is a better method for its robustness and sub-pixel accuracy. Moreover, by comparing the highest peak and the second highest peak in the power spectra of each pattern, we can detect oscillations with dubious frequency such as those caused by interference of nearby droplets.

3.2 Algorithm for two-frame tracking

The goal of the two-frame tracking algorithm is to match the droplets found in two consecutive image frames. The velocity of matched droplets can then be calculated using the droplet displacement and the known time interval between the frames. This is a similar problem to general particle tracking, but is much simpler because every droplet has a unique identity: its size.

The two-frame tracking algorithm developed here is specifically for particles of known size. The input to the algorithm is two sets of particle position and size data, found in the double-exposed images. For every particle in the first frame, its neighbors (within a user-defined radius) are found in the same frame, and its match candidates which have similar size and are within a certain shift are found in the second frame. A search is done to find particles with only one candidate. The matched particles are then removed from the candidate lists of all particles. This process is repeated until no new match is found.

After size match there may still exist unmatched particles with more than one candidate. For such particles the local motion of neighboring matched particles is used to help find the match. Since the magnitude of velocity can vary much greatly due to a wide range of sizes present, we assume that the direction of neighboring droplet motion should be similar. Therefore, a motion match that searches the match candidates only along the local flow direction was implemented. The local flow motion can also be used to detect outliers for both the size match and motion match sub-processes.

4. Measurement Capability

4.1 Sizing accuracy

Monodisperse droplets were used extensively to verify the sizing accuracy of the system. The monodisperse droplets were generated using a Vibrating Orifice Aerosol Generator (VOAG) and distilled water. Figure 5 shows the distribution of measured diameter of over 600 droplets (from 30 images). The mean measured diameter has less than 1% deviation from the expected diameter of 118.76 um.

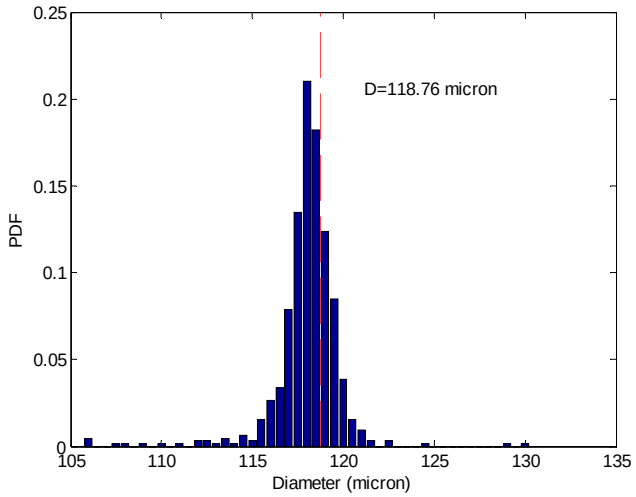

Figure 5: Measured diameter distribution of monodisperse droplets of 118.76 μm.

We also used 127 micron optical fiber to check the sizing accuracy (and the geometric correction method) at different locations in the field of view. The fiber was not simply clad, but rather had a graded index type construction. The refractive index varied from 1.467 at the center of the core to 1.45 at the core/cladding interface. The refractive index of the cladding was 1.45. Table 1 shows the measured fiber diameter at five locations in the field of view, from the extreme left to the extreme right. It is apparent that the system is fully capable of obtaining an accurate measurement of the fiber diameter (average error of 2.72%) and the geometric correction is limiting variation within the image to only ±1.5%.

Position (mm)	-7.5	-2.5	0	2.5	7.5
Diameter (μm)	127	128	128	129	130

Table 1: Measured diameter of a 127 micron optical fiber at five locations in the field of view

4.2 Size range

Theoretically the minimum oscillation spacing is two pixels and the maximum is equal to the width of the oscillation patterns (out-of-focus image of the droplet). This corresponds respectively to the maximum and minimum droplet diameter that can be measured by the system. Using geometric optics, we can obtain the following equations for the measurable size range:

$$d_{\min} = \lambda \cdot (1 + 1/M) \cdot f\#/A;\ d_{\max} = \lambda \cdot dz/(M \cdot \delta \cdot B) \quad (3)$$

where A is the minimum number of oscillations and $A \geq 1$; B is the minimum oscillation spacing in pixels and $B \geq 2$. Considering the noise present in real images, we use A = 1.5 and B = 3 to calculate the measurable size range of our system. Figure 6 shows the size range versus defocusing shift (translation of the camera assembly) at three pre-defocusing magnifications. Please note that since dz and M vary across the image, Figure 6 indicates the size range that can be measured regardless of droplets location. The actual size range may be wider if we separately consider droplets near the sides of the images.

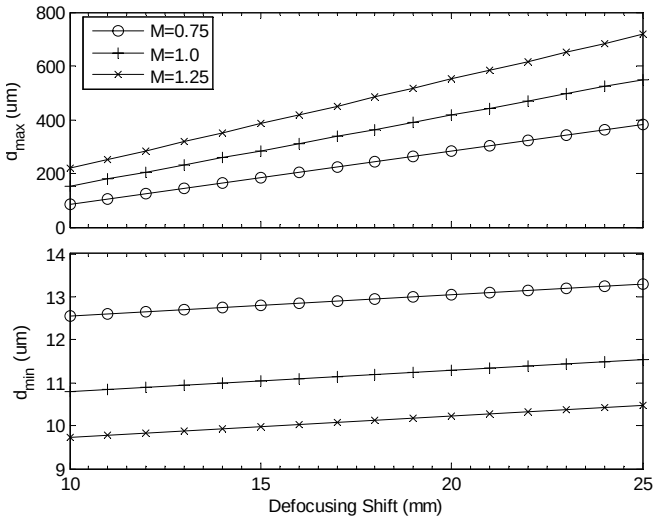

Figure 6: Measurable size range versus defocusing shift at three pre-defocusing magnifications

4.3 Droplet concentration

The use of a slit in our recording setup drastically reduces the possibility of oscillation pattern overlap, thus increasing the maximum limit in measurable number density. However, the relatively large size of out-of-focus images means image overlap is inevitable especially when droplet concentration is high, because overlap also can occur at the ends of the oscillation patterns. To explore the upper limit of droplet concentration that can be measured by our system, we used simulated out-of-focus images to calculate the percentage of overlapping droplets. As shown in Figure 7, when the concentration is 3 droplets per mm^3, about 55% of the droplets overlap with one or more droplets by up to 25% of its width. At a concentration of 10 droplets per mm^3 (10,000 #/cc), almost all droplets overlap. Based on our experience with the sizing algorithm, 3 droplets per mm^3 (3000 #/cc) is the maximum droplet concentration at which our system can give good results.

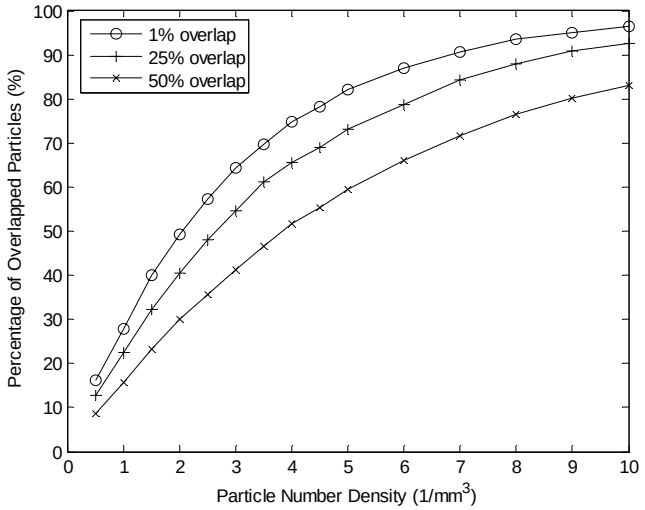

Figure 7: Percentage of overlapping droplets versus droplet concentration. Defocusing shift of 15 mm and pre-defocusing magnification of 1 are assumed.

5. Results and Discussion

5.1 Pressure Atomizer: Water

A commercial pressure atomizer (Delavan, type W) with a nominal angle of 60° and orifice diameter of 0.21 mm was used in tests to generate a realistic spray. The nominal flow rate of the nozzle was 1.89 liter/h at 0.86 MPa. The nozzle was operated with water at three pressure settings, ranging from 0.6 MPa to 0.8 MPa. Thus, the flow rate during the tests varied by about 10% from 1.6 liter/h at 0.6 MPa to 1.8 liter/h at 0.8 MPa. The spray was injected in air at 0.1 MPa environment pressure. Images were obtained at nine locations in 10 mm increments: six on-axis (x = 0) and three off axis. The field of view was 17 mm square, thus the overlap was about 40%. The light sheet thickness was set to about 250um using 500mm and 1000mm spherical lenses and a single −50mm cylindrical lens. A total of 40 image pairs were acquired at each location, yielding about 2000 diameter measurements. The distribution of droplets is shown in Figure 8. Each point corresponds to a droplet detected and measured by the system. What is most striking about this figure is the detail present near the nozzle, including the spray angle, since the technique was able to detect and measure droplets all the way up the spray nozzle.

Shown in Figure 9 is the size distribution in nine areas defined in Figure 8. The important trends of this atomizer were detected very well by the system. The sensitivity of our windowed FFT based approach is apparent in region A, where a population of smaller drops is detected among the more dominant group of larger droplets.

Near the nozzle, we see a dual peaked histogram, with larger drops ($d \approx 45$ μm) being generated in the spray sheet area, and the smaller drops ($d \approx 15$ μm) in the recirculating zone. As we move downstream, the peak corresponding to smaller drops increases because at y = 20~30 mm the field of view contains only the recirculating zone. As we move further down, the larger droplets peak becomes dominant, since the hollow cone closes at that location with the 0.6 MPa injection pressure used here. Then, moving in the x direction at y = 50 mm, we see a strong peak at about 45 μm, which corresponds to the actual sheet region of the spray plume. Interestingly, the trajectory of these droplets can be traced back up to the injector through region A, in Figure 8.

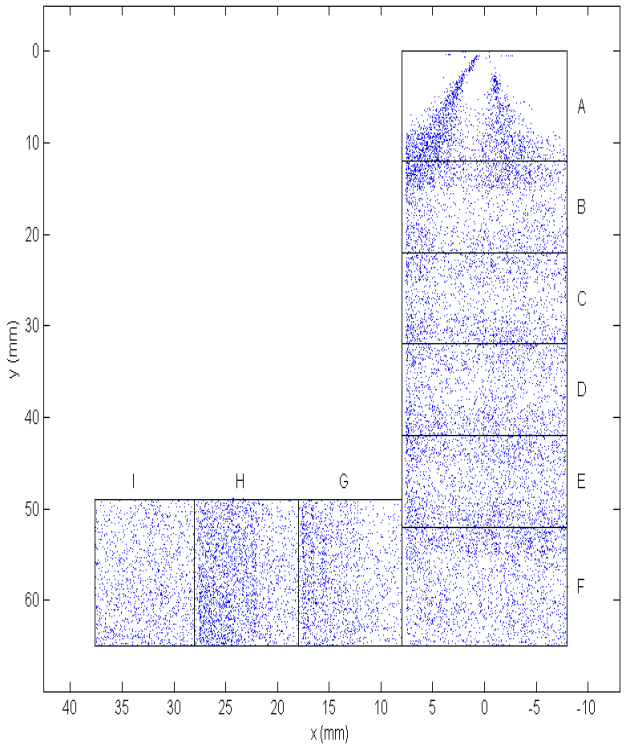

Figure 8: Distribution of measured droplets.

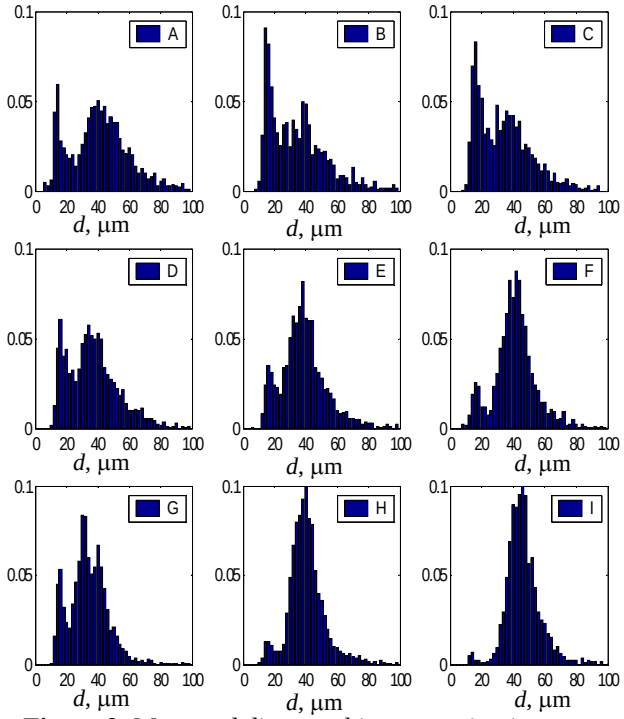

Figure 9: Measured diameter histograms in nine non-overlapping areas defined in Figure 8; P = 0.6 MPa.

The increase of pressure resulted in a significant variation of the spray structure as qualified in Figure 10, in which each point again corresponds to a droplet detected and

measured by the system. The blue and red dots represent droplets belonging to the large and small droplet groups, respectively, which were observed in the bimodal diameter distribution. As expected for swirl type pressure atomizers, the angle of the spray cone tends to increase with pressure. The spray generated by "W" nozzles is neither truly hollow nor solid (semi-solid cone). Figure 10 clearly shows this

Droplet velocities are also measured simultaneously. First the average velocity of spray plume is obtained from the velocities of individual droplets. Figure 12 shows the velocity map on a regular grid with interval Δx = 1 mm and Δy = 5 mm.

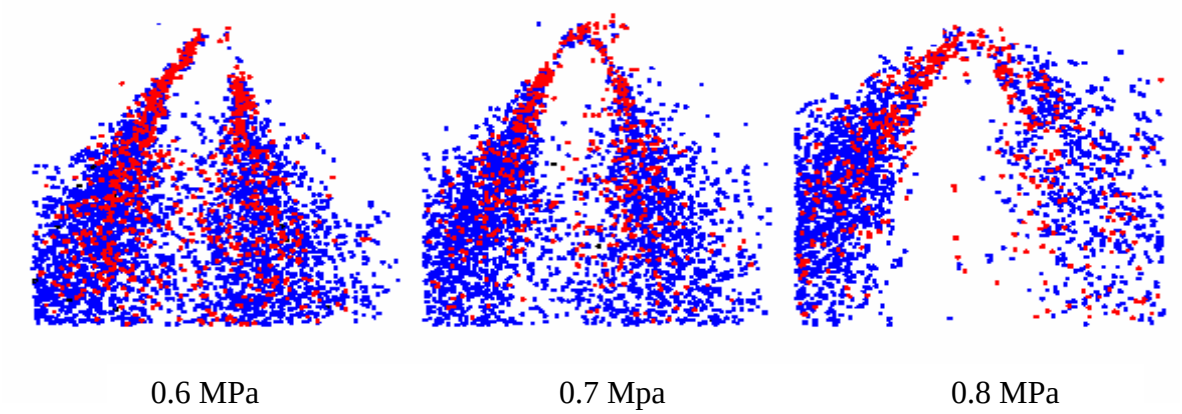

Figure 10: Spatial droplet distribution in the spray for different atomization pressures. Blue indicates a large drop and red indicates a small drop.

feature and, in addition, it appears that when increasing the pressure the empty internal zone of the spray increases, thus resulting in a spray structure more similar to the hollow-cone type. However, no significant differences were observed in the droplet size distributions measured at 0.8 MPa (Fig, 11).

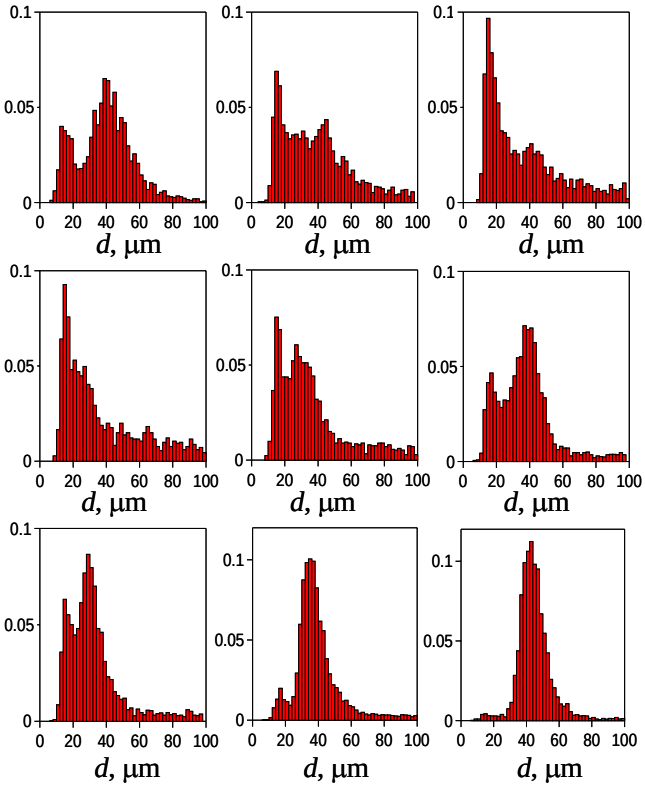

Figure 11: Measured diameter histograms in nine non-overlapping areas defined in Figure 8; P = 0.8 MPa.

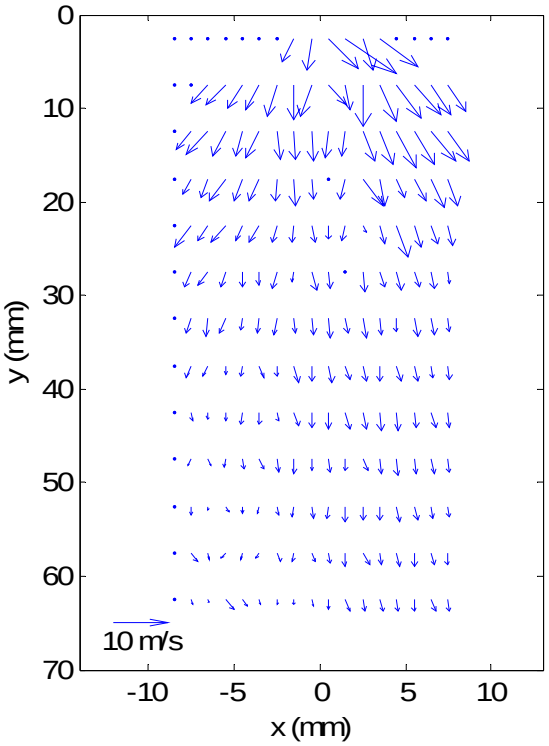

Figure 12: Average velocity of spray flow.

5.2 Pressure Atomizer: Fuel Oil

Shown in Figure 13 is the size distribution for the same Delavan pressure atomizer operating on fuel oil at a pressure of 0.6 MPa. The spray was injected in air at 0.1 MPa environment pressure. Data are shown for the location x=0 mm and y=0 mm. For comparison, the diameter histogram is also shown for water at the same spatial location. The important trends of this atomizer were again detected very well by the system. Although the refractive

index for fuel oil is typically about 1.45 compared to 1.33 for water, the GSI technique is insensitive to refractive index variations and so this value was not changed in the software.

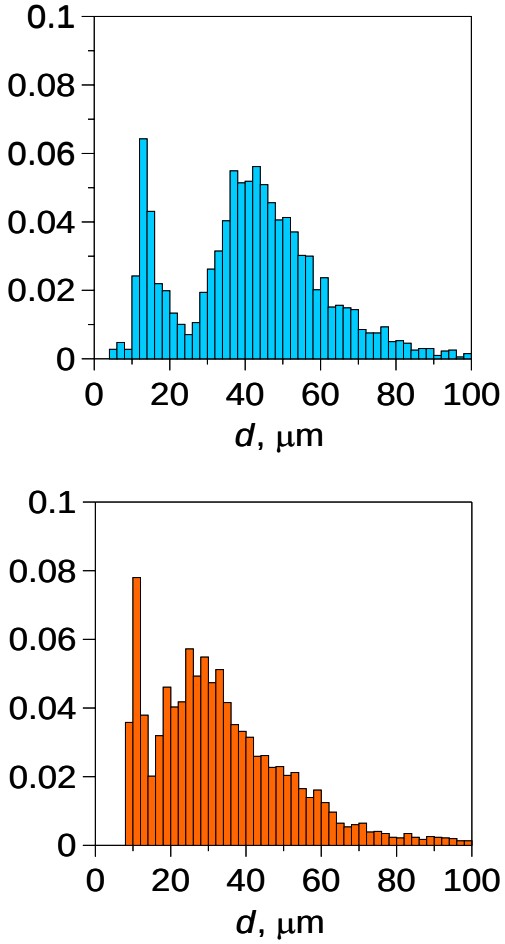

Figure 13: Diameter histogram for water (top) and fuel oil (bottom) sprays near the nozzle (spatial location A).

5.2 G-DI Spray: n-heptane substitute

Further measurements were performed on a gasoline direct injection (G-DI) spray system, spraying into the ambient atmosphere. This spray developed as a hollow cone with a separate cluster of droplets exiting mainly along the centerline at the start of injection, likely due to residual fuel in the orifice region. The cone part of the spray developed a leading edge roll-up vortex. Shown in Figure 14 is a bubble plot indicating droplet size and location for the G-DI spray operating on a gasoline substitute at a pressure of 0.9MPa. The top of this plot is 13 mm downstream from the nozzle, and the left edge of this plot is at the injector centerline. It is apparent from the figure that the spray travels down and to the right.

Figures 15, 16, 17 show diameter distributions for a plane through the nozzle centerline, 2mm away from the centerline, and 4mm from the centerline, respectively. Comparing these histograms, one can see that the peak and maximum diameters are increasing as we move away from the nozzle centerline. Overall, however, smaller droplet sizes are indicated here compared to the pressure atomizer, even though the applied pressure is only at a start-up level. Very few droplets have diameters above 100um. This is shown by the trend in SMD with distance from the centerline, shown in Fig. 18. The important trends of this atomizer were detected very well by the GSV system, in spite of the highly dense spray plume.

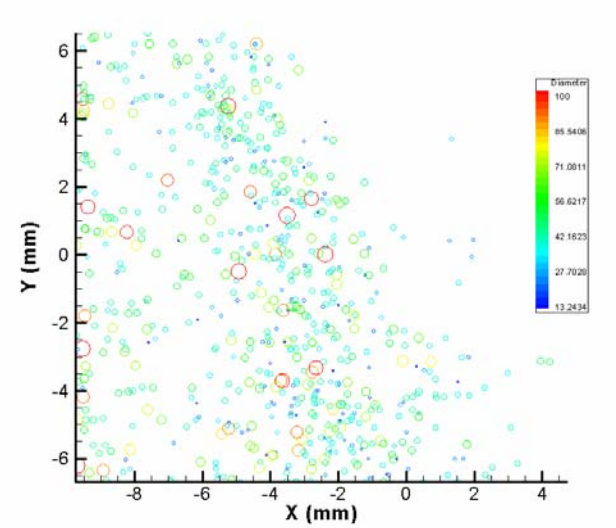

Figure 14: Droplet size and location for G-DI spray.

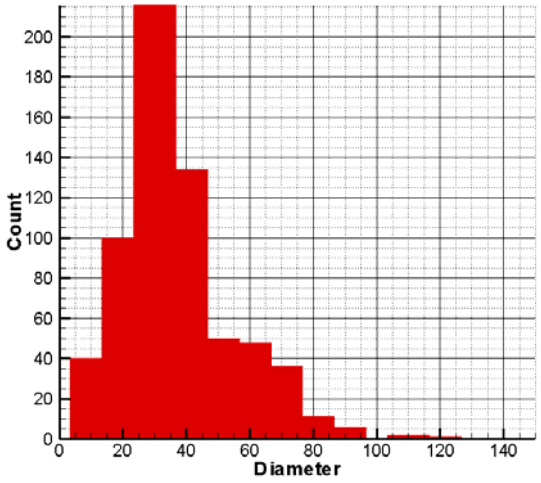

Figure 15: Diameter distribution for G-DI spray at location x=8.7 mm, y = 13 mm, and z= 0 (on-axis).

6. Conclusions

A new global droplet size and velocity measurement system has been developed using the GSI approach, with the capability to measure the velocity and size of droplets with non-uniform and/or varying refractive index. The windowed FFT based approach together with the optimized frequency-based algorithm was shown to extract the droplet size accurately and robustly. The two-frame tracking algorithm was employed to measure the velocity of droplets from the two consecutive image frames. The size range and droplet concentration limits were investigated using simulated out-of-focus images. The measurable diameter range for the system was verified to be from 10μm to 600μm for the range of magnification and defocus recommended here. The maximum droplet concentration was expected to be about 3000 #/cc.

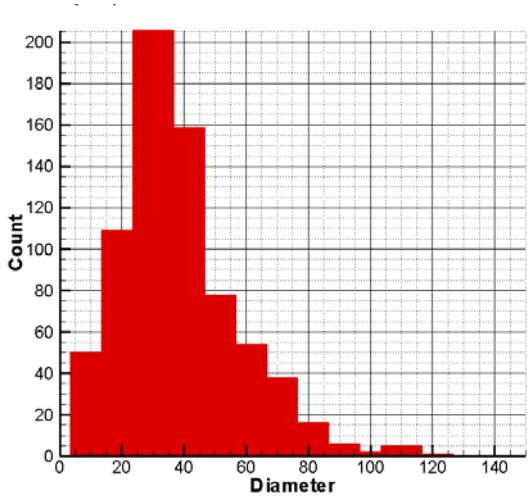

Figure 16: Diameter distribution for G-DI spray at location x=8.7 mm, y=13 mm, and z=2 mm (off-axis).

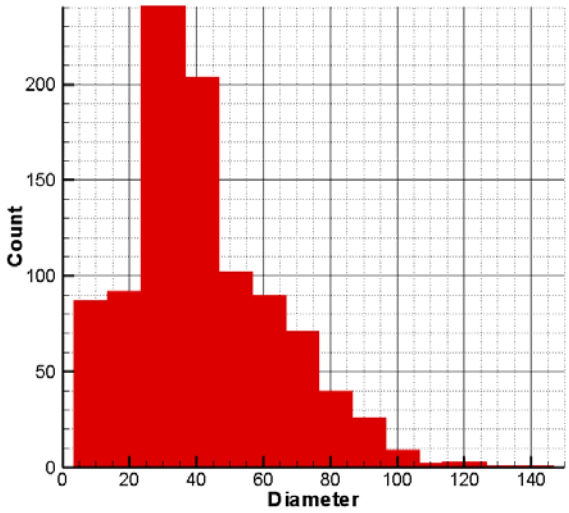

Figure 17: Diameter distribution for G-DI spray at location x=8.7 mm, y=13 mm, and z=4 mm (off-axis).

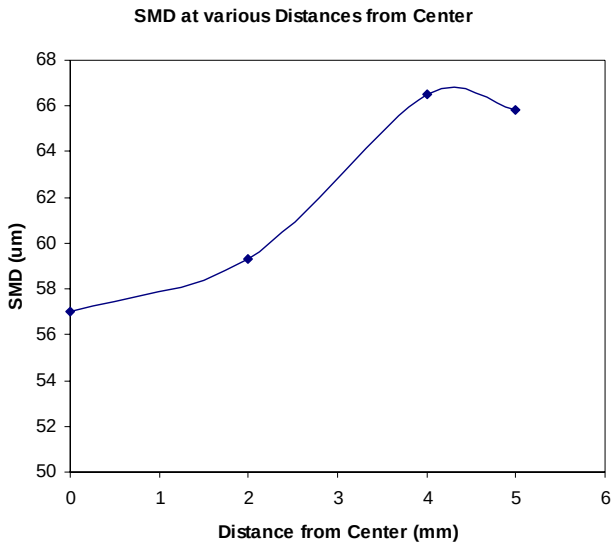

Figure 18: Sauter Mean Diameter as a function of distance from the nozzle centerline.

Sizing accuracy was verified using monodisperse droplets and a graded index optical fiber.

Data were obtained for a swirl type pressure atomizer operating on water and fuel oil. Results depicted well the near-nozzle spray angle and diameter characteristics in various parts of the spray structure. The water spray had generally larger droplet sizes compared to the fuel oil spray. Variation in fluid pressure from 0.6 MPa to 0.8 MPa caused a dramatic variation in spray angle and spray structure. Recirculation and spray sheet zones could easily be identified in the data, by the relative population of small and large droplets. Velocity vector maps were obtained, and combined with the size measurements, size-velocity correlations were constructed. These depicted the well-known trend of increasing velocity with droplet size.

Measurements of a G-DI spray were possible with the GSV system. These measurements revealed several interesting trends, including an increasing SMD as the measurement plane was traversed away from the centerline.

References

1. M. Kerker (1969) “The Scattering of Light and Other Electromagnetic Radiation”, Academic Press, New York, p175 (1969)
2. R. Ragucci, A. Cavaliere, P. Massoli (1990) “Drop Sizing by Laser Light Scattering Exploiting Intensity Angular Oscillation in the Mie Regime”, Particle and Particle Systems Characterization 7, pp221-225
3. P. Massoli, R. Calabria (1999) “Sizing of Droplets in Reactive Sprays by Mie Scattering Imaging”, 15th Conference on Liquid Atomization and Spray Systems, ILASS-Europe, July 5th-7th, Toulouse, France
4. K. Li, P. Massoli (1994) “Scattering of Electromagneticplane Waves by Radially Inhomogeneous Spheres: a Finely Stratifies Sphere Model”, Applied Optics 33, pp501-511
5. R. Calabria, A. Casaburi and P. Massoli (2003) “Improved GSI Out-of-Focus Technique for Application to Dense Sprays and PIV Measurements”, 9th Int. Conf. on Liquid Atomization and Spray Systems - ICLASS 2003, paper 10-6, Sorrento, Italy, July 13-17.
6. A. Glover, S. Skippon, R. Boyle (1995) "Interferometric laser imaging for droplet sizing: a method for droplet-size measurement in sparse spray systems", Applied Optics, v34 n36 pp8409-8421
7. A. Graβmann, F. Peters (2004) "Size Measurement of Very Small Spherical Particles by Mie Scattering Imaging (MSI)", Part. Part. Syst. Charact. v21 pp379-389
8. M. Maeda, T. Kawaguchi, K. Hishida (2000) "Novel interferometric measurement of size and velocity distributions of spherical particles in fluid flows", Measurement Science Technology, v11 L13-18
9. G. Pan, J. Shakal, W. Lai, R. Calabria, P. Massoli, “Simultaneous Global Size and Velocity Measurement of Droplets and Sprays”, 20th Conf. on Liquid Atomization and Spray Systems, ILASS-Europe, Orleans, France, 5th – 7th September, 2005, p.91-96.